Power Optimization for Integrated Active and Passive Sensing in DFRC Systems

Xingliang Lou, Wenchao Xia, *Member, IEEE*, Kai-Kit Wong, *Fellow, IEEE*, Haitao Zhao, *Senior Member, IEEE*, Tony Q. S. Quek, *Fellow, IEEE*, and Hongbo Zhu, *Member, IEEE*

Abstract

Most existing works on dual-function radar-communication (DFRC) systems mainly focus on active sensing, but ignore passive sensing. To leverage multi-static sensing capability, we explore integrated active and passive sensing (IAPS) in DFRC systems to remedy sensing performance. The multi-antenna base station (BS) is responsible for communication and active sensing by transmitting signals to user equipments while detecting a target according echo signals. Passive sensing is performed at the receive access points (RAPs). We consider both the cases where the capacity of the backhaul links between the RAPs and BS is unlimited and limited and adopt different fusion strategies. Specifically, when the backhaul capacity is unlimited, the BS and RAPs send sensing signals they received to the fusion center (FC) for signal fusion. The FC processes the signals and uses the generalized likelihood ratio test detector to determine if a target is present. However, when the backhaul capacity is limited, each RAP, as well as the BS, makes decisions independently and sends its binary inference results to the FC for result fusion via voting aggregation. Then, two power optimization algorithms are proposed to maximize the target detection probability under communication quality of service constraints. Finally, numerical simulations demonstrate that the sensing performance in the case of unlimited backhaul capacity is much better than that in the case of limited backhaul capacity, and the proposed IAPS scheme outperforms only-passive and only-active sensing schemes, especially when backhaul capacity is unlimited.

Index Terms

Dual-function radar-communication (DFRC), integrated sensing and communication, integrated active and passive sensing, fusion strategy, power allocation

X. Lou, W. Xia, and H. Zhu are with the Jiangsu Key Laboratory of Wireless Communications, Nanjing University of Posts and Telecommunications, Nanjing 210003, China, (e-mail: 2022010109@njupt.edu.cn, xiawenchao@njupt.edu.cn, zhuhb@njupt.edu.cn).

I. Introduction

Communication networks are evolving from 5G to 6G in pursuit of a network that achieves global coverage, green intelligence, sensory interconnection, and synesthesia integration [1]. To achieve this vision, besides the communication ability, environmental perception ability is also required. Electromagnetic wave has the ability to both sense environment and transmit data, but most existing works study and treat these two techniques independently, resulting in a conflict of wireless resources between sensing and communication systems. In order to improve frequency spectrum and hardware efficiency, researchers are recently considering the function integration of wireless communication and radar sensing, which promotes the research on dual-function radar-communication (DFRC) systems [2–4].

The primary idea behind DFRC systems is to share infrastructure and resources between communication and sensing functions, thereby combining radar sensing with wireless communication [5–8]. Recently, DFRC systems have garnered significant attention from both the academia and industry and there have been some works on the design and performance analysis of DFRC systems, e.g., [9–13]. Specifically, the feasibility of coexistence of multiple-input multiple-output (MIMO) radar and orthogonal frequency division multiplexing communication was demonstrated and transmit precoding was optimized to eliminate mutual interference between the radar and communication in [9]. [10] proposed two operational options. The first option involved sensing and communication each occupying a subset of antennas and the radar signal was designed to fall into the null space of downlink communication channel. The other option used a unified waveform for both radar and communication functions. In [11], the DFRC system transmitted the weighted sum of independent radar and communication symbols and formed multiple beams towards the target and the communication receivers. Different from [11], [12] proposed to jointly optimizing DFRC waveform and precoding matrix toward to realize sensing and communication functions simultaneously and the Cramér-Rao bound was used as a performance metric of target estimation. [13] designed a novel radar waveform for accurate estimations of timing offset and channel parameters. However, only signals of mono-static sensing transceiver was used in [9–13]. To improve the sensing accuracy, [14–16] attempted to make use of multiple signals for sensing. [14] proposed an uplink sensing scheme which jointly processed all measurements from spatial, temporal, and frequency domains for perceptive mobile networks with asynchronous transceivers. In [15], a base station (BS) working as a mono-static radar receiver was used to estimate angles-

of-arrival of targets based on itself downlink echo signals and uplink reflected signals from the users. To address self-interference problem of echo signal caused by the concurrent information transmission, [16] proposed to select one BS as a receiver to receive echo signals while other BSs act as transmitters.

Different from the above works which are based on mono-static sensing, recently multi-static sensing has attracted growing interests and is expected to bring various advantages over the conventional mono-static sensing. Multi-static sensing can not only reduce the mono-static sensing uncertainties caused by noise or incompleteness due to wireless fading and interference [17], but also provide better sensing coverage and capture richer sensing information [18]. There are only a few works on multi-static sensing in DFRC systems. In [19], a centralized federated processing method was proposed for the information received at multiple receive access points (RAPs) in a cell-free massive multiple-input multiple-output (MIMO) system. [20] attempted to improve sensing accuracy of human-sized objects by increasing the number of receive devices under indoor cellular deployment. [21] utilized a set of distributed transmitters which sent individual information and multiple sensing receivers to estimate the target. Assuming time synchronization among BSs in [22], each BS can exploit reflected signals of itself and other BSs for joint detection. [23] proposed to fuse the outputs of multiple dual-function radars to achieve higher sensing performance, but the communication and sensing signals were sent in different time slots in [23]. Despite the above progress, these previous works still suffer from many limitations. First of all, although multi-static sensing provides enhanced sensing capability, we note that most existing works focus on active sensing in DFRC systems and ignore the potential performance gain from passive sensing. In multi-static sensing, we refer to the sensing operation based on echo signals as active sensing, whereas the sensing operation based on the received signals from other transmitters (such as BSs and RAPs) as passive sensing. Secondly, challenges are still presented in terms of wireless resource allocation to properly balance the performance between sensing and communication. Finally, direct transmission of multi-static sensing signals to a fusion center (FC) for centralized processing leads to high communication overhead. But, the channel links to the FC are often capacity-limited.

Motivated by the analysis above, we aim to improve sensing performance by integrated active and passive sensing (IAPS) in DFRC systems without sacrificing communication performance. Specifically, BSs are responsible for communication as well as active sensing by transmitting signals to user equipments (UEs) while simultaneously detecting targets according to echo

signals. RAPs do not transmit signals to UEs but they can achieve reflected signals. To leverage the multi-static sensing capability and to address the uncertainty in sensing due to the fading and interference characteristics of wireless communication, we explore the performance gain of passive sensing performed at RAPs based on reflected signals they received. Considering the capacity of backhaul links between BSs and RAPs are usually limited, it is hard for each RAP to send its observation (i.e., reflected signals they received) directly to BSs or a FC. This practical consideration poses a challenge on the integration of active and passive sensing. In this work, we consider both the cases with unlimited and limited backhaul capacity and propose different fusion strategies. The contributions of this work are summarized as follows:

1) We consider a DFRC system where a BS communicates with UEs and senses a target simultaneously. Multiple RAPs are connected to the BS via backhaul links. In addition to active sensing signals received at the BS, passive sensing signals received at the RAPs are also exploited and then the IAPS scheme is proposed to improve sensing performance under communication quality-of-service (QoS) constraints. Furthermore, we consider two cases, i.e., one with unlimited backhaul capacity and the other with limited backhaul capacity, and propose power optimization algorithms, respectively.
2) In the case where the backhaul capacity is unlimited, the BS and RAPs send sensing signals they received to the FC for signal fusion. The FC processes the received signals and uses the generalized likelihood ratio test (GLRT) detector to determine if a target is present. Moreover, we proposed a power allocation algorithm to maximize the detection probability for improving sensing performance.
3) In the case where backhaul capacity is limited, the BS and RAPs make decisions based on their observation independently and send binary inference results to the FC for result fusion. A whitening filter is adopted to eliminate direct path interference [24]. Upon receiving active and passive sensing binary inference results, the FC performs voting aggregation to determine whether the target exists. We convert the probability of error minimization into a maximization problem of joint detection probability and propose a heuristic power optimization algorithm.
4) Finally, numerical simulations in the cases with unlimited and limited backhaul capacity are conducted. Numerical results demonstrate that the sensing performance in the case of unlimited backhaul capacity is much better than that in the case of limited backhaul

capacity. It is also observed that the performance of the proposed IAPS scheme is better than that of only-active and only-passive sensing scheme especially when backhaul capacity is unlimited. Besides, we find that the overall performance can be improved by increasing the numbers of RAPs.

The structure of this paper is given as follows. Firstly, Section II presents the system model. Then, Sections III and IV formulate the sensing performance optimization problems with communication QoS constraints in the cases where the backhaul capacity is unlimited and limited, respectively, and then propose corresponding power allocation algorithms. Numerical results are provided and discussed in Section V. Finally, Section VI concludes this paper.

Notation: Matrices and vectors are represented by bold uppercase and lowercase symbols, respectively. $\mathbb{E}[\cdot]$ denotes the expectation operator. $\mathrm{diag}(\cdot)$ and $\mathrm{blkdiag}(\cdot)$ stand for the construction of a diagonal matrix and the construction of a block diagonal matrix, respectively. $\|\cdot\|_1$ and $\|\cdot\|_2$ represent l_1 and l_2 norm, respectively. $\mathrm{tr}(\cdot)$ and $\mathrm{vec}(\cdot)$ denote the trace and the vectorization operations, respectively. $\mathfrak{R}(\cdot)$ and $\mathfrak{I}(\cdot)$ denote the real and imaginary parts of the argument. $(\cdot)^T$ and $(\cdot)^H$ stand for transpose and Hermitian transpose of the matrices, respectively. $\mathbf{I}$ is the identity matrix. $\lceil\cdot\rceil$ denotes the ceiling function.

II. System Model

A. System Setting

We consider a downlink DFRC system, as depicted in Fig. 1, where a BS equipped with M transmit antennas and N_0 receive antennas is response for serving K single-antenna UEs and detecting a single target simultaneously. There are also R RAPs each with N_1 receive antennas, which can be used to receive the reflected signals for sensing. Here, we refer to the sensing operation at the BS and RAPs as active and passive sensing, respectively. Note that $K \leq M$ is required to ensure the feasibility of downlink multi-user MIMO communications and $M < N_0$ is typically required to avoid the loss of information about the target [12]. Besides, a FC is introduced to process both the active and passive sensing signals. For notation convenience, we denote the set of UEs and the set of RAPs by $\mathcal{K} = \{1, 2, \ldots, K\}$ and $\mathcal{R} = \{1, 2, \ldots, R\}$, respectively. The BS is indexed using 0 and the set of the BS and RAPs are denoted by $\mathcal{R}' = \mathcal{R} \bigcup \{0\}$, Besides, the target is indexed using 0 and the set of UEs and target are denoted by $\mathcal{K}' = \mathcal{K} \bigcup \{0\}$.

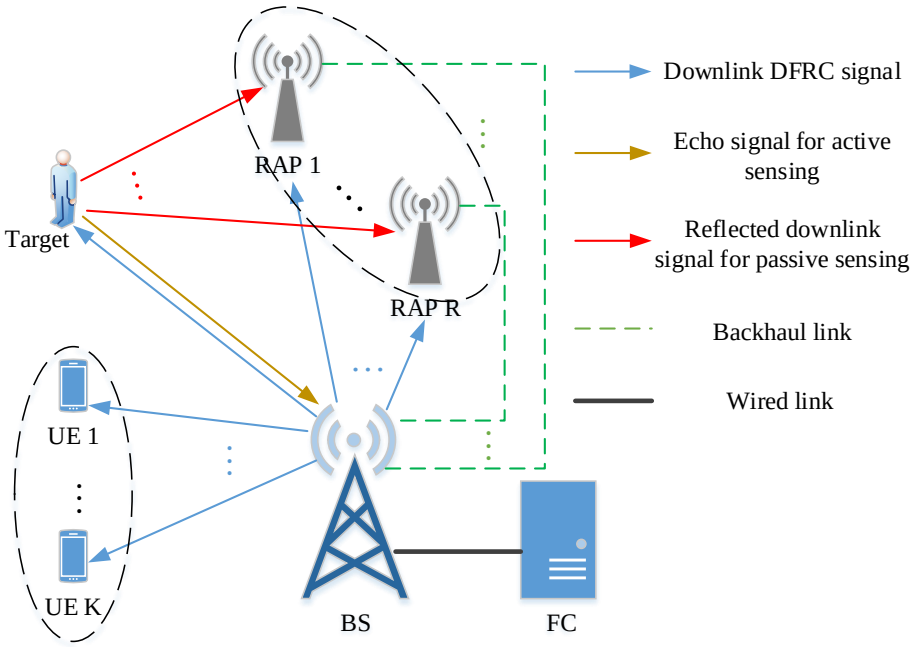

Fig. 1. The snapshot of a DFRC system.

Define $\mathbf{s}_0 \in \mathbb{C}^{L\times 1}$ as the dedicated sensing symbol vector and $\mathbf{s}_k \in \mathbb{C}^{L\times 1}$ as the communication symbol vector of the k-th UE, respectively. It is assumed that the sensing and communication symbols are independent of each other with $\frac{1}{L}\mathbb{E}\{\mathbf{S}\mathbf{S}^H\} = \mathbf{I}_{K+1}$, where $\mathbf{S} = [\mathbf{s}_0, \mathbf{s}_1, ..., \mathbf{s}_K]$. Then, the DFRC signal matrix is given as $\mathbf{X} = \mathbf{W}\mathbf{S}$, where

$$\mathbf{W} = [\sqrt{p_0}\tilde{\mathbf{w}}_0, \sqrt{p_1}\tilde{\mathbf{w}}_1, ..., \sqrt{p_K}\tilde{\mathbf{w}}_K] \in \mathbb{C}^{M\times(K+1)}, \tag{1}$$

where p_k and $\tilde{\mathbf{w}}_k, k \in \mathcal{K}'$ are the transmit power and the normalized precoding vector of targer and the k-th UE, respectively, with $||\tilde{\mathbf{w}}_k||_2 = 1$.

B. Communication Model

The received signal in the l-th communication symbol at the k-th UE is given as

$$y_k[l] = \mathbf{h}_k^H \sum_{k'=1}^{K} \sqrt{p_{k'}}\tilde{\mathbf{w}}_{k'} s_{k'}[l] + \sqrt{p_0}\mathbf{h}_k^H \tilde{\mathbf{w}}_0 s_0[l] + n_k[l], \tag{2}$$

where $n_k[l] \sim \mathcal{CN}(0, \sigma_{\mathrm{n}}^2)$ denotes the additive Gaussian white noise (AWGN) with zero mean and variance σ_{n}^2 and $\mathbf{h}_k$ denotes the channel between the k-th UE and the BS, which is assumed to be flat Rayleigh fading and statistically independent of each other.

Then, the signal to interference plus noise ratio (SINR) of the k-th UE is given by

$$\gamma_k = \frac{p_k |\mathbf{h}_k^H \tilde{\mathbf{w}}_k|^2}{\sum_{k'=1, k' \neq k}^{K} p_{k'} |\mathbf{h}_k^H \tilde{\mathbf{w}}_{k'}|^2 + p_0 |\mathbf{h}_k^H \tilde{\mathbf{w}}_0|^2 + \sigma_{\mathrm{n}}^2}. \tag{3}$$

C. Sensing Model

The BS can sense the target through the echo signal, which is given as

$$\mathbf{z}_0[l] = \alpha_0 \mathbf{b}_0(\theta) \mathbf{a}^H(\theta) \mathbf{X}[l] + \mathbf{n}_0'[l] \in \mathbb{C}^{N_0 \times 1}, \tag{4}$$

where $\mathbf{n}_0'[l] \sim \mathcal{CN}(\mathbf{0}, \sigma_{\mathrm{n}}^2 \mathbf{I}_{N_0})$ denotes the AWGN vector, $\mathbf{X}[l]$ represents the l-th column of $\mathbf{X}$, $\alpha_0 \sim \mathcal{CN}\left(0, \sigma_{\mathrm{rcs}}^2\right)$ is the combined sensing channel gain that includes the path-loss through target and the radar cross section (RCS) of the target [25], and θ is the azimuth angle of target relative to the antenna array at the BS. The transmit and receive steering vectors of the BS are denoted by

$$\mathbf{a}(\cdot) = \left[1, e^{j2\pi\Delta \sin(\cdot)}, \ldots, e^{j2\pi(M-1)\Delta \sin(\cdot)}\right]^T \in \mathbb{C}^{M \times 1}, \tag{5}$$

$$\mathbf{b}_0(\cdot) = \left[1, e^{j2\pi\Delta \sin(\cdot)}, \ldots, e^{j2\pi(N_0-1)\Delta \sin(\cdot)}\right]^T \in \mathbb{C}^{N_0 \times 1}, \tag{6}$$

respectively, where Δ is the spacing between adjacent antennas normalized by wavelength.

When a target is present, the reflected sensing signal received at the r-th RAP for passive sensing is given as

$$\mathbf{z}_r[l] = \alpha_r \mathbf{b}_1(\varphi_r) \mathbf{a}^H(\theta) \mathbf{X}[l] + \mathbf{G}_r \mathbf{X}[l] + \mathbf{n}_r'[l] \in \mathbb{C}^{N_1 \times 1}, \tag{7}$$

where $\mathbf{n}_r'[l] \sim \mathcal{CN}(\mathbf{0}, \sigma_{\mathrm{n}}^2 \mathbf{I}_{N_1})$ denotes the AWGN vector, $\alpha_r \sim \mathcal{CN}(0, \sigma_{\mathrm{rcs}}^2)$ is the combined sensing channel gain, φ_r is the azimuth angle of target relative to the r-th RAP, $\mathbf{G}_r \in \mathbb{C}^{N_1 \times M}$ represents the target-free channel between the BS and the r-th RAP, and $\mathbf{b}_1(\cdot)$ is the steering vector of the RAPs, given as

$$\mathbf{b}_1(\cdot) = \left[1, e^{j2\pi\Delta \sin(\cdot)}, \ldots, e^{j2\pi(N_1-1)\Delta \sin(\cdot)}\right]^T \in \mathbb{C}^{N_1 \times 1}, \tag{8}$$

D. Transmit Precoding Vectors

The transmit precoding is designed based on the regularized zero-forcing (RZF) scheme, i.e., $\tilde{\mathbf{w}}_k = \bar{\mathbf{w}}_k / \|\bar{\mathbf{w}}_k\|_2$ with

$$\bar{\mathbf{w}}_k = (\mathbf{H}\mathbf{H}^H + \lambda \mathbf{I}_M)^{-1}\mathbf{h}_k, \tag{9}$$

where $\mathbf{H} = [\mathbf{h}_1, \mathbf{h}_2, ..., \mathbf{h}_K] \in \mathbb{C}^{M\times K}$ and λ is the regularization parameter.

In order to eliminate the interference caused by sensing symbols to the UEs, we employ the zero-forcing radar (ZFR) precoder $\tilde{\mathbf{w}}_0 = \bar{\mathbf{w}}_0 / \|\bar{\mathbf{w}}_0\|_2$ [26], where

$$\bar{\mathbf{w}}_0 = (\mathbf{I}_M - \mathbf{H}\mathbf{H}^H)^{-1}\mathbf{a}(\theta). \tag{10}$$

The BS and RAPs are connected through the backhaul channel using wired or wireless links. In this work, we conduct analysis in two cases, i.e., unlimited and limited backhaul capacity. Specifically, when the backhaul capacity is unlimited (such as fiber links), both the BS and RAPs directly sends the received sensing signals to the FC for joint processing, which will be introduced in Section III. However, when the backhaul capacity is limited (such as wireless links), it is impractical for the RAPs to send the sensing signal directly due to the large amount of sensing signals. As an alternative solution, each RAP first make decisions independently and then send binary inference results to the FC for voting aggregation, such that only a few bits are needed to exchange. More details about the latter solution will given in Section IV.

III. DFRC System With Unlimited Backhaul Capacity

In this section, we assume the backhaul capacity is unlimited, thus the BS and RAPs can directly send the received sensing signals to the FC for joint processing.

A. Active and Passive Sensing Signal Fusion

With the unlimited backhaul capacity, it is reasonable to assume $\mathbf{X}$ and $\mathbf{G} = [\mathbf{G}_0, \mathbf{G}_1, ..., \mathbf{G}_R]$ are known at the FC, which can be estimated using the method proposed in [27]. Therefore, the target-free portion of the received sensing signal at the RAPs can be mitigated perfectly. Then, $\mathbf{z}_r$ in (7) can be rewritten as

$$\mathbf{z}_r[l] = \alpha_r \mathbf{A}_r[l] + \mathbf{n}'_r[l], \tag{11}$$

where $\mathbf{A}_r[l] = \mathbf{b}_1(\varphi_r)\,\mathbf{a}^H(\theta)\,\mathbf{X}[l]$ is the known part at the FC.

We collect the received sensing signals at the BS and RAPs into a vector $\mathbf{z}[l] = \left[\mathbf{z}_0^T[l] \dots \mathbf{z}_R^T[l]\right]^T$, and the overall sensing signal is expressed as

$$\mathbf{z}[l] = \mathbf{A}[l]\boldsymbol{\alpha} + \mathbf{n}'[l] \in \mathbb{C}^{(N_0+RN_1)\times 1}, \tag{12}$$

where $\boldsymbol{\alpha} = [\alpha_0, \alpha_1, ..., \alpha_R]^T$ is a collection of the unknown sensing channel coefficients, $\mathbf{n}'[l] = \left[\mathbf{n}_0'^T[l] \dots \mathbf{n}_R'^T[l]\right]^T$ is the concatenated noise, and $\mathbf{A}[l]$ is the known part and is given as

$$\mathbf{A}[l] = \text{blkdiag}(\mathbf{A}_0[l], \mathbf{A}_1[l], ..., \mathbf{A}_R[l]) \in \mathbb{C}^{(N_0+RN_1)\times(R+1)}. \tag{13}$$

B. GLRT Detector

Here, the received signals in L communication time slots are used for detection. We define the vectors $\mathbf{z}_L \in \mathbb{C}^{(N_0+RN_1)L\times 1}$, $\mathbf{n}'_L \in \mathbb{C}^{(N_0+RN_1)L\times 1}$, and $\mathbf{A}'_L \in \mathbb{C}^{(N_0+RN_1)L\times 1}$, which are constructed by concatenating $\mathbf{z}[l]$, $\mathbf{n}'[l]$, and $\mathbf{A}[l]\boldsymbol{\alpha}$, respectively, i.e.,

$$\mathbf{z}_L = \left[\mathbf{z}^T[1] \dots \mathbf{z}^T[L]\right]^T, \tag{14}$$

$$\mathbf{n}'_L = \left[\mathbf{n}'^T[1] \dots \mathbf{n}'^T[L]\right]^T. \tag{15}$$

and

$$\mathbf{A}'_L = \left[[\mathbf{A}[1]\boldsymbol{\alpha}]^T \dots [\mathbf{A}[L]\boldsymbol{\alpha}]^T\right]^T, \tag{16}$$

The binary hypothesis used in the GLRT detector is written as

$$\begin{cases} \mathcal{H}_0 : \mathbf{z}_L = \mathbf{n}'_L, \\ \mathcal{H}_1 : \mathbf{z}_L = \mathbf{A}'_L + \mathbf{n}'_L. \end{cases} \tag{17}$$

Then the corresponding GLRT detector is given by

$$\Lambda = \frac{\max_{\boldsymbol{\alpha}} f(\mathbf{z}_L|\boldsymbol{\alpha}, \mathcal{H}_1)}{f(\mathbf{z}_L|\mathcal{H}_0)} \underset{\mathcal{H}_0}{\overset{\mathcal{H}_1}{\gtrless}} \xi, \tag{18}$$

where ξ is the threshold of the GLRT detector, which is selected to achieve a desired false alarm probability P_{FA} under Neyman-Pearson criterion [28]. The joint probability density function (PDF) of the overall received sensing signal in cases $\mathcal{H}_1$ and $\mathcal{H}_0$ is computed as [29]

$$f(\mathbf{z}_L|\boldsymbol{\alpha}, \mathcal{H}_1) = \frac{1}{(\pi\sigma_{\text{n}}^2)^{(R+1)L}} \cdot \exp[-\sum_{l=1}^{L} \frac{(\mathbf{z}[l] - \mathbf{A}[l]\boldsymbol{\alpha})^H(\mathbf{z}[l] - \mathbf{A}[l]\boldsymbol{\alpha})}{\sigma_{\text{n}}^2}], \tag{19}$$

$$f(\mathbf{z}_L|\mathcal{H}_0) = \frac{1}{(\pi\sigma_{\rm n}^2)^{(R+1)L}} \cdot \exp(-\sum_{l=1}^{L} \frac{\mathbf{z}[l]^H \mathbf{z}[l]}{\sigma_{\rm n}^2}), \tag{20}$$

respectively. We note that maximizing $f(\mathbf{z}_L|\boldsymbol{\alpha}, \mathcal{H}_1)$ with respect to $\boldsymbol{\alpha}$ is equivalent to

$$\min_{\boldsymbol{\alpha}} \sum_{l=1}^{L} \frac{(\mathbf{z}[l] - \mathbf{A}[l]\boldsymbol{\alpha})^H (\mathbf{z}[l] - \mathbf{A}[l]\boldsymbol{\alpha})}{\sigma_{\rm n}^2}, \tag{21}$$

which in turn is equivalent to

$$\max_{\boldsymbol{\alpha}} 2\Re\{\boldsymbol{\alpha}^H \Big(\sum_{l=1}^{L} \frac{\mathbf{A}^H[l]\mathbf{z}[l]}{\sigma_{\rm n}^2} \Big)\} - \boldsymbol{\alpha}^H \Big(\sum_{l=1}^{L} \frac{\mathbf{A}^H[l]\mathbf{A}[l]}{\sigma_{\rm n}^2} \Big) \boldsymbol{\alpha}. \tag{22}$$

Thus, $\boldsymbol{\alpha}$ can be estimated as

$$\hat{\boldsymbol{\alpha}} = \Big(\sum_{l=1}^{L} \mathbf{A}^H[l]\mathbf{A}[l] \Big)^{-1} \Big(\sum_{l=1}^{L} \mathbf{A}^H[l]\mathbf{z}[l] \Big). \tag{23}$$

Inserting the estimated $\hat{\boldsymbol{\alpha}}$ into the GLRT detector, we obtain the test statistic as

$$\ln(\Lambda) = \frac{1}{\sigma_{\rm n}^2} (\sum_{l=1}^{L} \mathbf{z}^H[l]\mathbf{A}[l]) (\sum_{l=1}^{L} \mathbf{A}^H[l]\mathbf{A}[l])^{-1} (\sum_{l=1}^{L} \mathbf{A}^H[l]\mathbf{z}[l]) \underset{\mathcal{H}_0}{\overset{\mathcal{H}_1}{\gtrless}} \ln(\xi). \tag{24}$$

According to [28], the asymptotic distribution of (24) can be expressed as

$$\ln(\Lambda) \sim \begin{cases} \mathcal{H}_1 : \mathcal{X}_2^2(\rho), \\ \mathcal{H}_0 : \mathcal{X}_2^2, \end{cases} \tag{25}$$

where $\mathcal{X}_2^2$ and $\mathcal{X}_2^2(\rho)$ are central and non-central chi-squared distributions with two Degrees of Freedom (DoFs), respectively, and ρ is the non-central parameter. When the GLRT is used, the threshold ξ can be expressed as

$$\xi = \mathfrak{F}_{\mathcal{X}_2^2}^{-1} \left(1 - P_{\rm FA}\right), \tag{26}$$

and the detection probability $P_{\rm D}$ is given as [30]

$$P_{\rm D} = 1 - \mathfrak{F}_{\mathcal{X}_2^2(\rho)}(\xi), \tag{27}$$

where $\mathfrak{F}_{\mathcal{X}_2^2(\rho)}$ is the non-central chi-square Cumulative Distribution Function (CDF) with two DoFs.

Because different RCSs are assumed to be independent and have zero mean, we have

$$\begin{aligned}\mathbb{E}\{\mathbf{A}[l]\boldsymbol{\alpha}\boldsymbol{\alpha}^H\mathbf{A}^H[l]\} &= \mathbb{E}\{\text{blkdiag}(|\alpha_0|^2\,\mathbf{A}_0[l]\mathbf{A}_0[l]^H, ..., |\alpha_R|^2\,\mathbf{A}_R[l]\mathbf{A}_R[l]^H)\} \\ &= \sigma_{\text{rcs}}^2\text{blkdiag}(\mathbf{B}_0\hat{\mathbf{W}}\mathbf{B}_0^H, ..., \mathbf{B}_R\hat{\mathbf{W}}\mathbf{B}_R^H), \end{aligned} \tag{28}$$

where $\hat{\mathbf{W}} = \mathbf{W}\mathbf{W}^H$, $\mathbf{B}_0 = \mathbf{b}_0(\theta)\,\mathbf{a}^H(\theta)$, and $\mathbf{B}_r = \mathbf{b}_1(\varphi_r)\,\mathbf{a}^H(\theta)$. Then, the non-centrality parameter ρ is given as

$$\begin{aligned}\rho &= \sum_{l=1}^{L}\text{tr}\left(\mathbb{E}\{\mathbf{A}[l]\boldsymbol{\alpha}\boldsymbol{\alpha}^H\mathbf{A}^H[l]\}(\mathbb{E}\{\mathbf{n}_L'\})^{-1}\right) \\ &= \frac{L\sigma_{\text{rcs}}^2}{L(N_0+RN_1)\sigma_{\text{n}}^2}\,\text{tr}\left(\text{blkdiag}(\mathbf{B}_0\hat{\mathbf{W}}\mathbf{B}_0^H, ..., \mathbf{B}_R\hat{\mathbf{W}}\mathbf{B}_R^H)\right) \\ &= \frac{\sigma_{\text{rcs}}^2}{(N_0+RN_1)\sigma_{\text{n}}^2}\sum_{r=0}^{R}\text{tr}\left(\mathbf{B}_r\hat{\mathbf{W}}\mathbf{B}_r^H\right). \end{aligned} \tag{29}$$

C. Problem Formulation

The goal is to maximize the detection performance under SINR constraints of the UEs and a power constraint of the BS, which is formulated as

$$\begin{aligned}\mathcal{P}_0: \max_{\mathbf{p}\geq\mathbf{0}}\ & P_{\text{D}} \\ \text{s.t. } & \gamma_k \geq \Gamma, k \in \mathcal{K}, && \text{(30a)} \\ & ||\mathbf{p}||_1 \leq P_{\max}, && \text{(30b)}\end{aligned}$$

where $\mathbf{p} = [p_0, p_1, ..., p_K]^T$, Γ is the minimum SINR threshold for the UEs, and $P_{\max}$ is the power budget of the BS. It is observed that P_{D} is a monotonically increasing function with respect to ρ [28] and $\frac{\sigma_{\text{rcs}}^2}{(N_0+RN_1)\sigma_{\text{n}}^2}$ is a constant. Therefore, problem $\mathcal{P}_0$ can be equivalently formulated as

$$\begin{aligned}\mathcal{P}_1: \max_{\mathbf{p}\geq\mathbf{0}}\ & \sum_{r=0}^{R}\text{tr}\left(\mathbf{B}_r\hat{\mathbf{W}}\mathbf{B}_r^H\right) \\ \text{s.t. } & \text{(30a) and (30b).}\end{aligned}$$

According to the properties of matrix trace, we have

$$\begin{aligned}\mathrm{tr}\left(\mathbf{B}_r\hat{\mathbf{W}}\mathbf{B}_r^H\right) &= \mathrm{tr}\left(\hat{\mathbf{W}}\mathbf{B}_r^H\mathbf{B}_r\right)\\ &= \mathrm{tr}\left(\mathrm{diag}(\mathbf{p})\tilde{\mathbf{W}}^H\mathbf{B}_r^H\mathbf{B}_r\tilde{\mathbf{W}}\right),\end{aligned} \tag{31}$$

where $\tilde{\mathbf{W}} = [\tilde{\mathbf{w}}_0, \tilde{\mathbf{w}}_1, ..., \tilde{\mathbf{w}}_K]$. Since $\tilde{\mathbf{W}}^H\mathbf{B}_r^H\mathbf{B}_r\tilde{\mathbf{W}}$ is a Hermitian symmetric matrix where the elements on the diagonal must be real, i.e., $\mathrm{tr}\left(\Im\{\tilde{\mathbf{W}}^H\mathbf{B}_r^H\mathbf{B}_r\tilde{\mathbf{W}}\}\right) = 0, \forall\mathbf{p}$. The QoS constraints can be rewritten in the form of second-order cone (SOC) as [19]

$$\left\|[\varrho_{k,0}\sqrt{p_0},\ \varrho_{k,1}\sqrt{p_1},\ \ldots,\ 0,\ \ldots,\ \varrho_{k,K}\sqrt{p_K},\ \sigma_{\mathrm{n}}]\right\|_2 \leq \frac{\sqrt{p_k}\varrho_{k,k}}{\sqrt{\Gamma}}, k = 1, \ldots, K, \tag{32}$$

where $\varrho_{k,j} = \left|\mathbf{h}_k^H\tilde{\mathbf{w}}_j\right|$. Now, problem $\mathcal{P}_1$ is reformulated as

$$\begin{aligned}\mathcal{P}_2 : \min_{\mathbf{p}\geq\mathbf{0}} & -\sum_{r=0}^{R}\mathrm{tr}\left(\mathrm{diag}(\mathbf{p})\Re\{\tilde{\mathbf{W}}^H\mathbf{B}_r^H\mathbf{B}_r\tilde{\mathbf{W}}\}\right)\\ \text{s.t. } & \text{(30b) and (32)}.\end{aligned}$$

Now, $\mathcal{P}_2$ becomes a standard Semidefinite Program (SDP) which can be solved using optimization tools, such as CVX [31].

IV. DFRC System With Limited Backhaul Capacity

When the backhaul capacity is limited, the RAPs cannot directly send the reflected signals they received. Instead, they independently make decisions based on their own observation and then send binary inference results to the FC for result fusion via voting aggregation.

A. GLRT Detector

Since the backhaul capacity is limited and the RAPs have to make decisions locally, the interference to the sensing signal at the RAPs from the BS via the target-free channel cannot be ignored. Then, the binary hypothesis is described as:

$$\begin{cases}\mathcal{H}_0 : \mathbf{z}_r[l] = \mathbf{G}_r\mathbf{X}[l] + \mathbf{n}_r'[l],\\ \mathcal{H}_1 : \mathbf{z}_r[l] = \alpha_r\mathbf{B}_r\mathbf{X}[l] + \mathbf{G}_r\mathbf{X}[l] + \mathbf{n}_r'[l].\end{cases} \tag{33}$$

For simplicity, we assume that the RAPs have accurately estimated the interference-plus-noise covariance matrix [24]. We use the GLRT detector to solve the unknown parameters α_r, φ_r and

θ. In order to consider the sufficient statistic of received signal, a matching filter is adopted [32], i.e.,

$$\begin{aligned}\tilde{\mathbf{Z}}_r &= \frac{1}{\sqrt{L}}\sum_{l=1}^{L}\mathbf{z}_r[l]\mathbf{X}^H[l] \\ &= \alpha_r\sqrt{L}\mathbf{B}_r\hat{\mathbf{W}} + \frac{1}{\sqrt{L}}(\mathbf{G}_r\mathbf{X}+\mathbf{n}_r')\mathbf{X}^H. \end{aligned} \tag{34}$$

Define $\tilde{\mathbf{z}}$ as the vectorization of $\tilde{\mathbf{Z}}$, which is given as

$$\begin{aligned}\tilde{\mathbf{z}}_r &= \mathrm{vec}(\tilde{\mathbf{Z}}_r) \\ &= \alpha_r\sqrt{L}\mathrm{vec}(\mathbf{B}_r\hat{\mathbf{W}}) + \boldsymbol{\varepsilon}_r, \end{aligned} \tag{35}$$

where $\boldsymbol{\varepsilon}_r = \frac{1}{\sqrt{L}}\mathrm{vec}((\mathbf{G}_r\mathbf{X}+\mathbf{n}_r')\mathbf{X}^H)$ is zero-mean, complex Gaussian distributed, and has the following block covariance matrix:

$$\mathbf{C}_r = \begin{bmatrix} \mathbf{Q}_r+\sigma_{\mathrm{n}}^2\mathbf{I}_{N_1} & & \mathbf{0} \\ & \cdots & \\ \mathbf{0} & & \mathbf{Q}_r+\sigma_{\mathrm{n}}^2\mathbf{I}_{N_1} \end{bmatrix} \in \mathbb{C}^{N_1M\times N_1M}, \tag{36}$$

where $\mathbf{Q}_r = \mathbf{G}_r\hat{\mathbf{W}}\mathbf{G}_r^H$.

Before using the GLRT detector, we apply a whitening filter to $\boldsymbol{\varepsilon}_r$. Specifically, considering that $\mathbf{C}_r$ is a positive-definite Hermitian matrix, the Cherosky decomposition is adopted as $\mathbf{C}_r^{-1} = \mathbf{U}_r\mathbf{U}_r^H$, where $\mathbf{U}_r$ is the lower triangle matrix. Then, $\mathbf{U}_r^H$ is used as the whitening filter in (33),

$$\begin{cases} \mathcal{H}_0 : \tilde{\mathbf{z}}_r = \mathbf{U}_r^H\boldsymbol{\varepsilon}_r, \\ \mathcal{H}_1 : \tilde{\mathbf{z}}_r = \alpha_r\sqrt{L}\mathbf{U}_r^H\mathbf{d}(\varphi_r,\theta) + \mathbf{U}_r^H\boldsymbol{\varepsilon}_r, \end{cases} \tag{37}$$

where $\mathbf{d}(\varphi_r,\theta) = \mathrm{vec}(\mathbf{B}_r\hat{\mathbf{W}})$. Thus, the corresponding GLRT detector is given by

$$\Delta_r = \frac{\max_{\alpha_r,\varphi_r,\theta} f(\tilde{\mathbf{z}}_r|\alpha_r,\varphi_r,\theta,\mathcal{H}_1)}{f(\tilde{\mathbf{z}}_r|\mathcal{H}_0)} \underset{\mathcal{H}_0}{\overset{\mathcal{H}_1}{\gtrless}} \zeta, \tag{38}$$

where $f(\tilde{\mathbf{z}}_r|\alpha_r,\varphi_r,\theta,\mathcal{H}_1)$ and $f(\tilde{\mathbf{z}}_r|\mathcal{H}_0)$ are the PDF under $\mathcal{H}_1$ and $\mathcal{H}_0$, respectively, and ζ is the decision threshold. For the given φ_r and θ, the maximum likelihood estimation (MLE) of α_r is obatined using the complex least-squares estimation and is given as

$$\hat{\alpha}_r = \frac{\mathbf{d}^H(\varphi_r,\theta)\mathbf{C}_r^{-1}\tilde{\mathbf{z}}_r}{\mathbf{d}^H(\varphi_r,\theta)\mathbf{C}_r^{-1}\mathbf{d}(\varphi_r,\theta)}. \tag{39}$$

By substituting (39) into (38), the MLE of $[\varphi_r, \theta]$ can be expressed as

$$[\hat{\varphi}_r, \hat{\theta}] = \arg\max_{\varphi_r,\theta} \frac{\left|\mathbf{d}^H(\varphi_r,\theta)\mathbf{C}_r^{-1}\tilde{\mathbf{z}}_r\right|^2}{\mathbf{d}^H(\varphi_r,\theta)\mathbf{C}_r^{-1}\mathbf{d}(\varphi_r,\theta)}. \tag{40}$$

Hence, the GLRT test statistic is expressed as

$$\begin{aligned}\ln(\Lambda_r) &= \frac{\left|\mathbf{d}^H(\hat{\varphi}_r,\hat{\theta})\mathbf{U}_r\mathbf{U}_r^H\tilde{\mathbf{z}}_r\right|^2}{\left\|\mathbf{U}_r^H\mathbf{d}(\hat{\varphi}_r,\hat{\theta})\right\|^2} \\ &= \frac{\left|\mathrm{tr}\left(\tilde{\mathbf{Z}}_r\hat{\mathbf{W}}^H\hat{\mathbf{B}}_r^H\tilde{\mathbf{Q}}_r^{-1}\right)\right|^2}{\mathrm{tr}\left(\hat{\mathbf{B}}_r\hat{\mathbf{W}}\hat{\mathbf{W}}^H\hat{\mathbf{B}}^H\tilde{\mathbf{Q}}_r^{-1}\right)} \underset{\mathcal{H}_0}{\overset{\mathcal{H}_1}{\gtrless}} \ln(\zeta),\end{aligned} \tag{41}$$

where $\tilde{\mathbf{Q}}_r = \mathbf{Q}_r + \sigma_{\mathrm{n}}^2\mathbf{I}_{N_1}$. The asymptotic distribution is expressed as

$$\ln(\Lambda_r) \sim \begin{cases} \mathcal{H}_1 : \mathcal{X}_2^2(\rho_r), \\ \mathcal{H}_0 : \mathcal{X}_2^2, \end{cases} \tag{42}$$

where the non-centrality parameter ρ_r of the r-th RAP is given as

$$\begin{aligned}\rho_r &= \mathbb{E}\{|\alpha_r|^2 L\,\mathrm{vec}^H(\mathbf{B}_r\hat{\mathbf{W}})\mathbf{C}_r^{-1}\,\mathrm{vec}(\mathbf{B}_r\hat{\mathbf{W}})\} \\ &= \sigma_{\mathrm{rcs}}^2 L\,\mathrm{tr}\left(\mathbf{B}_r\hat{\mathbf{W}}\hat{\mathbf{W}}^H\mathbf{B}_r^H\left(\mathbf{Q}_r + \sigma_{\mathrm{n}}^2\mathbf{I}_{N_1}\right)^{-1}\right).\end{aligned} \tag{43}$$

Besides, the non-centrality parameter ρ_0 of the BS is given as

$$\begin{aligned}\rho_0 &= \mathbb{E}\{|\alpha_0|^2 L\,\mathrm{vec}^H(\mathbf{B}_0\hat{\mathbf{W}})\mathbf{C}_0^{-1}\,\mathrm{vec}(\mathbf{B}_0\hat{\mathbf{W}})\} \\ &= \sigma_{\mathrm{rcs}}^2 L\,\mathrm{tr}\left(\mathbf{B}_0\hat{\mathbf{W}}\hat{\mathbf{W}}^H\mathbf{B}_0^H\left(\sigma_{\mathrm{n}}^2\mathbf{I}_{N_1}\right)^{-1}\right).\end{aligned} \tag{44}$$

Similar to (27), we can obtain the detection probability P_{D_r} of the r-th RAP as well as P_{D_0} of the BS.

B. Voting Aggregation

The FC performs voting aggregation when receiving the binary inference results from the RAPs and BS, which can be modeled by:

$$\begin{cases} \mathcal{H}_0 : \text{ No target}, \\ \mathcal{H}_1 : \text{Exist target}. \end{cases} \tag{45}$$

Then the voting rule is expressed as

$$\begin{cases} \mathcal{H}_0 : \sum_{r=0}^{R} D_r \leq \kappa, \\ \mathcal{H}_1 : \sum_{r=0}^{R} D_r \geq \kappa, \end{cases} \tag{46}$$

where D_r, $r \in \mathcal{R}'$ is the binary inference result, with $D_r = 0$ standing for no target and $D_r = 1$ standing for an existing target, κ represents the voting threshold. The probability of error at the FC is [33]

$$\Upsilon(\kappa, \hat{P}_{\mathrm{D}}) = \frac{1}{2} + \frac{1}{2} \sum_{i=0}^{\kappa-1} \binom{R+1}{i} \left[(\hat{P}_{\mathrm{D}})^i (1-\hat{P}_{\mathrm{D}})^{R+1-i} - (\hat{P}_{\mathrm{FA}})^i (1-\hat{P}_{\mathrm{FA}})^{R+1-i} \right], \tag{47}$$

where

$$\hat{P}_{\mathrm{D}} = \frac{1}{R+1} \sum_{r=0}^{R} P_{\mathrm{D}_r}, \tag{48}$$

$$\hat{P}_{\mathrm{FA}} = \frac{1}{R+1} \sum_{r=0}^{R} P_{\mathrm{FA}_r}, \tag{49}$$

P_{D_r} and P_{FA_r},$r \in \mathcal{R}'$ represent the detection probability and the false alarm probability, respectively, and

$$\binom{R+1}{i} = \frac{(R+1)!}{i!(R+1-i)!}. \tag{50}$$

The optimal κ is obtained as [33]

$$\tilde{\kappa} = \min \left(R+1, \left\lceil \frac{R+1}{1+\beta(\hat{P}_{\mathrm{D}})} \right\rceil \right), \tag{51}$$

where

$$\beta(\hat{P}_{\mathrm{D}}) = \frac{\ln \frac{\hat{P}_{\mathrm{FA}}}{\hat{P}_{\mathrm{D}}}}{\ln \frac{1-\hat{P}_{\mathrm{D}}}{1-\hat{P}_{\mathrm{FA}}}}. \tag{52}$$

C. Problem Formulation

We aim to minimize the probability of error at the FC, but the expression of $\Upsilon(\kappa, \hat{P}_{\mathrm{D}})$, as shown in (47), is quite complex. To handle this issue, we first introduce the following lemmas.

Lemma 1: Given $\hat{P}_{\mathrm{D}} \in (0,1)$, $\beta(\hat{P}_{\mathrm{D}})$ decreases as $\hat{P}_{\mathrm{D}}$ increases.

Proof: See Appendix A.

Lemma 2: Given $\hat{P}_{\mathrm{D}} \in (0,1)$, $\Upsilon(\tilde{\kappa}, \hat{P}_{\mathrm{D}})$ decreases as $\hat{P}_{\mathrm{D}}$ increases.

Proof: See Appendix B.

Based on **Lemma** 2, the minimization of the probability of error at the FC is equivalent to the maximization of $\hat{P}_{\mathrm{D}}$. Thus, the optimization problem is formulated as

$$\begin{aligned} \mathcal{P}_3: \ & \max_{\mathbf{p}\geq\mathbf{0}} \hat{P}_{\mathrm{D}} \\ & \text{s.t. } \gamma_k \geq \Gamma, k \in \mathcal{K}, \\ & ||\mathbf{p}||_1 = P_{\max}, \end{aligned}$$

which is a non-convex problem. Before giving the solution to problem $\mathcal{P}_3$, we first introduce the following lemma.

Lemma 3: When p_0 gradually increases and satisfies the transmit power constraint $||\mathbf{p}||_1 = P_{\max}$, $\hat{P}_{\mathrm{D}}$ gradually increases.

Proof: See Appendix C.

For further validation of **Lemma** 3, we plot the trend of $\hat{P}_{\mathrm{D}}$ with respect to p_0, as shown in Fig. 2. We first initialize $p_0 = 0$ and then gradually increase p_0 with a step size of Δp. After obtaining the power allocation vector, P_{D_r} and $\hat{P}_{\mathrm{D}}$ are calculated using (27) and (48), respectively. The simulation result in Fig. 2 is obtained averaging over 1000 samples, which is consistent with the conclusion in **Lemma** 3.

Based on **Lemma** 3, we propose a heuristic algorithm and summarize the proposed algorithm in Algorithm 1. Specifically, we decrease p_0 by Δp gradually and find the solution, $\mathbf{p}' = [p_1, p_2, \ldots, p_K]^T$, to the power minimization problem under the SINR constraints. Such a process is repeated until $\|\mathbf{p}\|_1 \leq P_{\max}$.

Algorithm 1 Proposed heuristic algorithm of power allocation.

1: Initialize $p_0' = P_{\max}$, the step size Δp, and $P_{\text{sum}} = p_0'$.
2: **while** $P_{\text{sum}} >= P_{\max}$ **do**
3: Set $p_0 = p_0' - \Delta p$.
4: Find solution to the following problem using SDP, i.e.,

$$\begin{cases} \min_{\mathbf{p}'} & \|\mathbf{p}\|_1 \\ \text{s.t.} & \gamma_k \geq \Gamma, \quad k \in \mathcal{K}. \end{cases}$$

5: Set $P_{\text{sum}} = \|\mathbf{p}\|_1$.
6: Set $p_0' = p_0$.
7: **end while**
8: Output: $\mathbf{p}$.

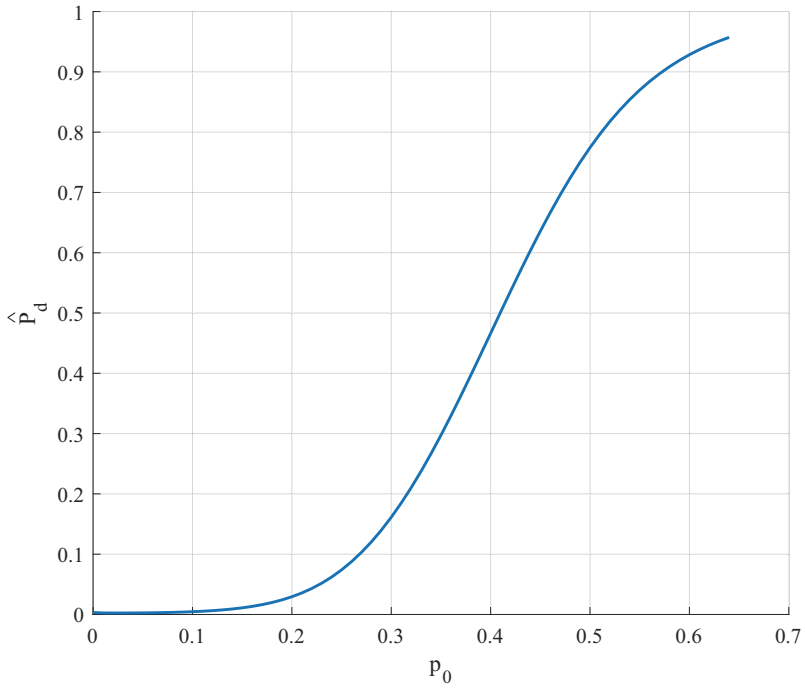

Fig. 2. The relation between $\hat{P}_{\mathrm{D}}$ and p_0 with $\{P_{\max}$ =1W, Γ =15dB$\}$.

V. Numerical Results

To evaluate the performance of the proposed DFRC system, we perform numerical simulations in a 500 m $\times$ 500 m region with a BS, $R = 10$ RAPs, and $K = 8$ UEs. The locations of the RAPs, UEs, and BS are randomly generated and the target is in the center of the region, as shown in Fig. 3. The BS and RAPs each is equipped with $N_0 = N_1$ = 20 receive antennas. Besides, the BS is equipped with M = 16 transmit antennas. Similar to [34], the channel model is generated using $\mathbf{h}_k = \sqrt{m_k}\tilde{\mathbf{h}}_k \in \mathbb{C}^{M\times 1}$, where $\tilde{\mathbf{h}}_k \sim \mathcal{CN}(\mathbf{0}, \mathbf{I}_M)$ is the small-scale fading and $m_k = 128.1 + 37.6\log_{10}(d)$ [dB] represents the path loss between the k-th UE and BS with d being the distance in kilometers. The target-free channel $\mathbf{G}$ is generated using the same channel model. The combined sensing channel gain of target is used the Swerling-I model [35]. The SINR threshold is set as $\Gamma = 15$ dB and the symbol number is set as L = 30. The detection threshold is determined by the false alarm probability $P_{\mathrm{FA}} = 10^{-5}$.

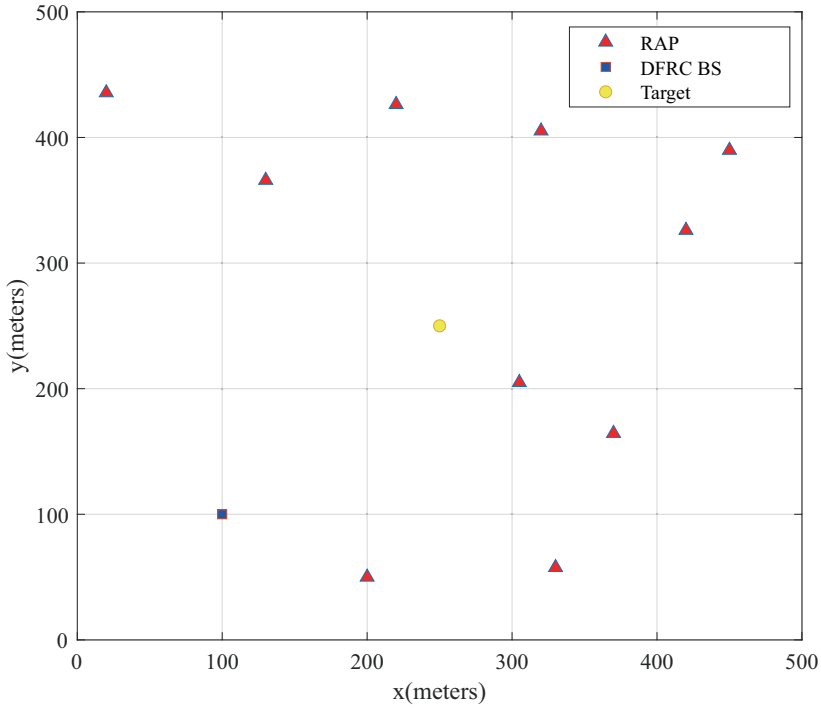

Fig. 3. The 2D locations of the RAPs, DFRC BS, and the target.

A. *Results with Unlimited Backhaul Capacity*

We first consider the case where the backhaul capacity is unlimited. Before presenting the numerical results, we first introduce the following baseline schemes for comparison.

1) Firstly, we find the solution to problem $\mathcal{P}_2$ considering the cases with and without dedicated sensing symbols (marked as "with s_0" and "w/o s_0", respectively).
2) Then, only-active and only-passive sensing schemes (marked as "active" and "passive", respectively) are introduced.
3) Finally, we also introduce the communication-centric scheme which aims to minimize the total power consumption (marked as "$\min P_{\text{total}}$") under the same constraints for comparison.

We evaluate these schemes using average detection probability, which is calculated by averaging over 1000 random samples. Fig. 4 shows that the average detection probability increases with the increase of σ_{rcs}^2. We find the proposed IAPS scheme with sensing symbols has the best performance, whose average detection probability can reach 1 when $\sigma_{\text{rcs}}^2 =$ -35 dB. The perfor-

mance of the only-passive sensing scheme is worse than that of the proposed IAPS scheme, but is much better than that of the only-active sensing scheme in both the cases with and without dedicated sensing symbols. This is because when the backhaul capacity is unlimited, all the RAPs can send the reflective signals they received to the FC and R observed signals can be utilized in the only-passive sensing scheme. However, only the echo signal received at the BS is utilized in the only-active sensing scheme. Besides, the average detection probability of the communication-centric scheme is almost 0 when $\sigma_{\text{rcs}}^2 \leq -7$ dB since the sensing requirement is not considered. We also observe that compared to the cases without dedicated sensing symbols, the average detection probability of difference schemes can be improved by using dedicated sensing symbols, which validates the importance of dedicated sensing symbols.

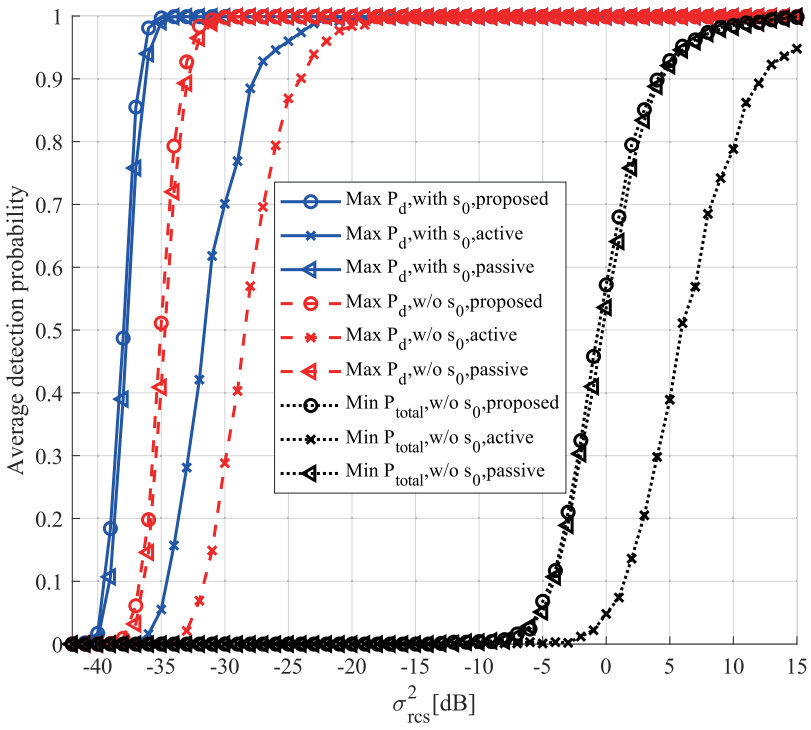

Fig. 4. The average detection probability vs. σ_{rcs}^2 with $P_{\max} = 1$ W.

Fig. 5 shows the average detection probability with respect to the transmit power budget of the BS $P_{\max}$. We find that the average detection probability can be improved with more available power. Consistent with the results in Fig. 4, the proposed IAPS scheme shows better performance than the other two schemes in both the cases with and without dedicated sensing symbols. Besides, with the advantage of quantity, the proposed scheme without dedicated sensing

symbols, as well as the only-passive sensing scheme without dedicated sensing symbols, shows better performance than the only-active sensing scheme with dedicated sensing symbols. This is because the communication symbols can also be used for target detection.

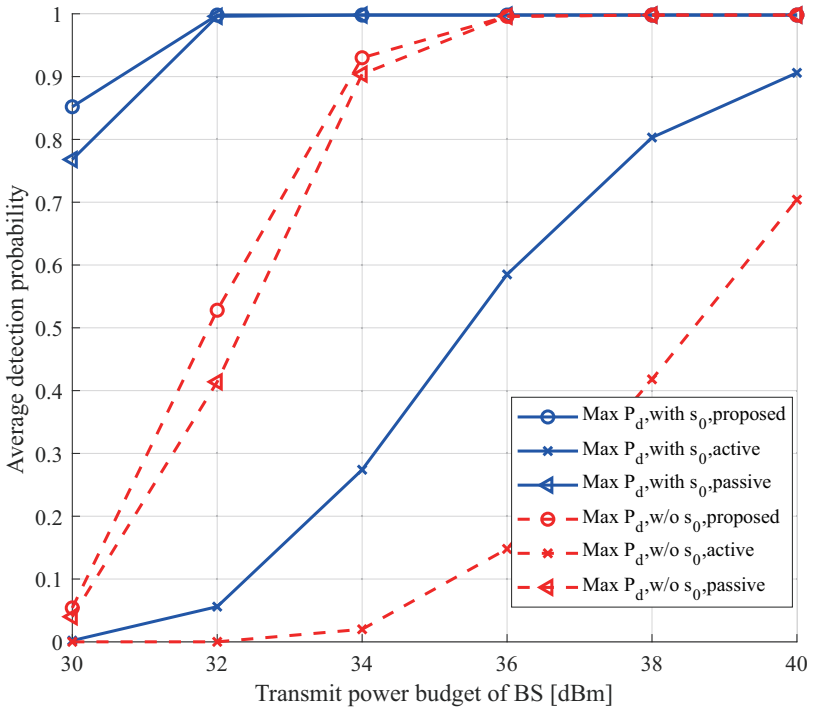

Fig. 5. The average detection probability vs. the transmit power budget of the BS $P_{\max}$ with $\sigma_{\text{rcs}}^2 = -37$dB.

Fig. 6 further shows the relationship between the average detection probability and the RAP number. The only-active sensing scheme is independent of the RAP number and thus is not presented in Fig. 6. It is observed that with the growth of the RAP number, the average detection probability of the proposed IAPS scheme, as well as the only-passive sensing scheme, gradually increases. This fact indicates that the FC gains more information as the RAP number increases. In addition, we find that the use of the dedicated sensing symbols allows a fast convergence rate, compared to the scheme without dedicated sensing symbols.

Fig. 7 illustrates the effect of the number of UEs on the average detection probability. We observe that the average detection probability of the schemes with dedicated sensing symbols gradually decreases as the UE number increases. This is because, with the fixed power budget $P_{\max}$ and the increase of the UE number, more power is allocated to meet user SINR constraints and less power is allocated to dedicated sensing symbols. However, in the case of without

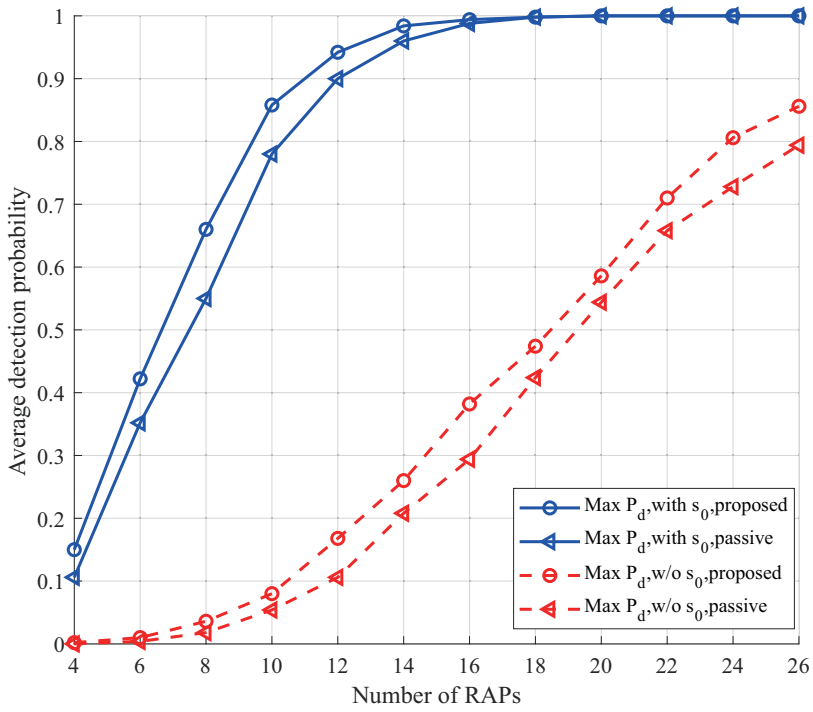

Fig. 6. The average detection probability vs. the number of RAPs with $\{\sigma_{\rm rcs}^2 = -37\text{dB},\ P_{\max} = 1\text{W}\}$.

dedicated sensing symbols as the UE number increases, the average detection probability of the proposed IAPS scheme, as well as the only-passive sensing scheme, increases first and then decreases. The reason behind this phenomenon is that a small increase of the UE number leads to more communication symbols used for sensing and further the increase of the average detection probability. However, when the UE number exceeds a threshold value (i.e., 6 in Fig. 7), more power is used to satisfy the increasing SINR constraints, which is not conducive to sensing performance.

B. Results with Limited Backhaul Capacity

We first introduce two labels, i.e., "unlimited" and "limited" to distinguish the two cases with unlimit and limited backhaul capacity. Fig. 8 shows that the average detection probability increases with the increase of $\sigma_{\rm rcs}^2$, regardless of whether backhaul capacity is unlimit or limited. We also observe that the achieved performance with the limited backhaul capacity is worse than that with the unlimited backhaul capacity because more sensing information is exploited in the case of unlimited backhaul capacity but only binary inference results is integrated in the

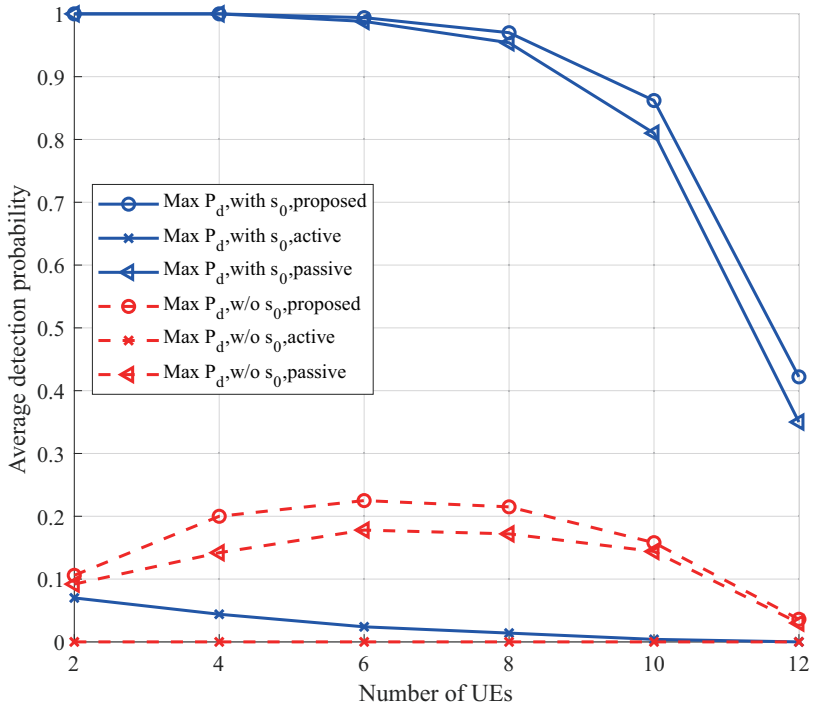

Fig. 7. The average detection probability vs. the number of UEs with $\{\sigma_{\text{rcs}}^2 = -36\text{dB}, P_{\max} = 1\text{W}\}$.

case of limited backhaul capacity. Similar to the results in (5), it is observed that the proposed IAPS scheme always achieves a higher average detection probability than that of the only-active and only-passive sensing schemes. Note that in the only-active sensing scheme, the influence of backhaul capacity can be ignored because no passive sensing is involved.

Fig. 9 shows the average detection probability with respect to the number of RAPs with different σ_{rcs}^2 values. The increase of the RAP number can reduce the probability of misjudgment after the voting aggregation. We note that the average detection probability increases as the number of the RAPs increases when $\sigma_{\text{rcs}}^2 \geq -36$ dB, but the curve with $\sigma_{\text{rcs}}^2 = -35\text{dB}$ rises faster than the curve with $\sigma_{\text{rcs}}^2 = -36\text{dB}$. In addition, we also find that when $\sigma_{\text{rcs}}^2 = -37\text{dB}$, the average detection probability is almost unchanged. This is because the voting aggregation at the FC highly depends on the binary inference results of each single RAP and the detection probability of each single RAP relies on σ_{rcs}^2.

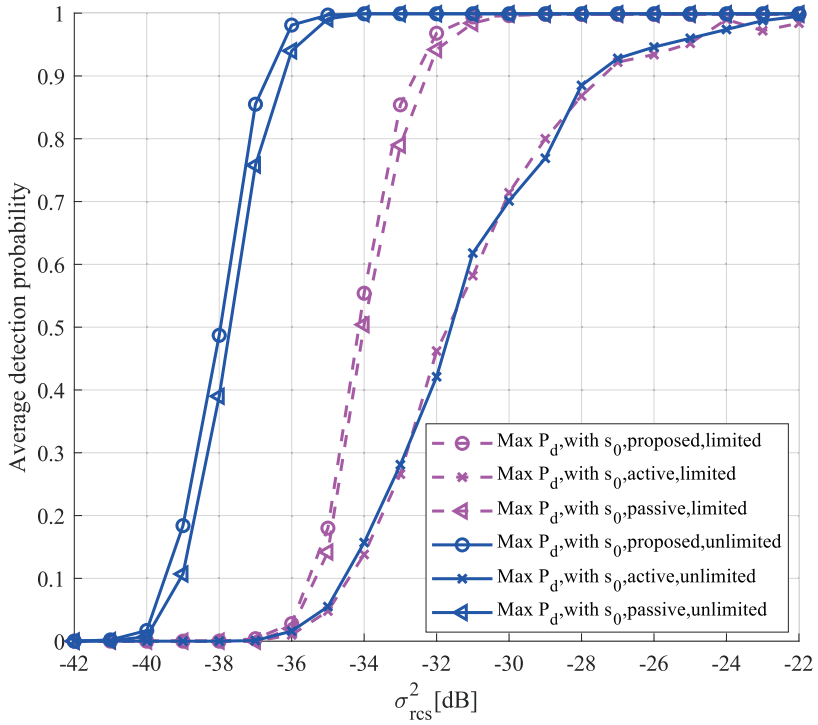

Fig. 8. The average detection probability vs. σ^2_{rcs}, $P_{\max} = 1$ W.

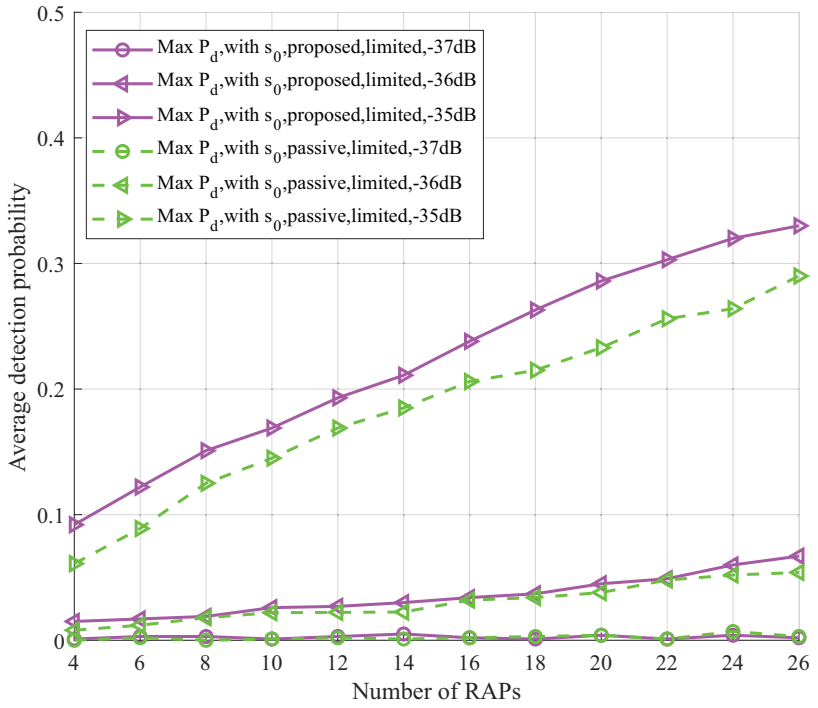

Fig. 9. The average detection probability vs. the number of RAPs, $P_{\max} = 1$ W.

VI. CONCLUSION

This paper considered a DFRC system and proposed IAPS scheme to improve sensing performance under communication QoS constraints. According to the backhaul capacity between RAPs and BS (i.e., limited or unlimited), different fusion schemes were adopted to exploit the active sensing and passive sensing information. Specifically, when the backhaul capacity is unlimited, the BS and RAPs send the sensing signal they received to the FC for signal fusion. The FC processes the signals and uses the GLRT detector to determine if a target is present. However, which the backhaul capacity is limited, the RAPs make decisions and send binary inference results to the FC for result fusion via voting aggregation. Different power allocation algorithms are designed to maximize the detection probability. Finally, numerical simulations in the cases with unlimited and limited backhaul capacity were conducted, which validated the performance gain of the proposed IAPS scheme and the positive effect of dedicated sensing symbols. Besides, we also found that the overall performance can be improved by increasing the number of RAPs.

APPENDIX

A. *Proof of* ***Lemma*** *1*

The derivative of $\beta(\hat{P}_{\mathrm{D}})$ is given as

$$\frac{\mathrm{d}\beta(\hat{P}_{\mathrm{D}})}{\mathrm{d}\hat{P}_{\mathrm{D}}}=\frac{(1-\hat{P}_{\mathrm{D}})(\ln(1-\hat{P}_{\mathrm{FA}})-\ln(1-\hat{P}_{\mathrm{D}}))+\hat{P}_{\mathrm{D}}(\ln\hat{P}_{\mathrm{FA}}-\ln\hat{P}_{\mathrm{D}})}{\hat{P}_{\mathrm{D}}(1-\hat{P}_{\mathrm{D}})(\ln(1-\hat{P}_{\mathrm{D}})-\ln(1-\hat{P}_{\mathrm{FA}}))^{2}}, \tag{53}$$

whose denominator is greater than 0. Define $\beta_1(\hat{P}_{\mathrm{D}})=(1-\hat{P}_{\mathrm{D}})(\ln(1-\hat{P}_{\mathrm{FA}})-\ln(1-\hat{P}_{\mathrm{D}}))+\hat{P}_{\mathrm{D}}(\ln\hat{P}_{\mathrm{FA}}-\ln\hat{P}_{\mathrm{D}})$. The first and second derivatives of $\beta_1(\hat{P}_{\mathrm{D}})$ are given as

$$\frac{\mathrm{d}\beta_1(\hat{P}_{\mathrm{D}})}{\mathrm{d}\hat{P}_{\mathrm{D}}}=-\ln(1-\hat{P}_{\mathrm{FA}})+\ln(1-\hat{P}_{\mathrm{D}})+\ln\hat{P}_{\mathrm{FA}}-\ln\hat{P}_{\mathrm{D}}, \tag{54}$$

and

$$\frac{\mathrm{d}^2\beta_1(\hat{P}_{\mathrm{D}})}{\mathrm{d}(\hat{P}_{\mathrm{D}})^2}=-\frac{1}{1-\hat{P}_{\mathrm{D}}}-\frac{1}{\hat{P}_{\mathrm{D}}}, \tag{55}$$

respectively. Note that (55) is less than 0 because of $\hat{P}_{\mathrm{D}}\in(0,1)$, which suggests that $\beta_1(\hat{P}_{\mathrm{D}})$ is a concave function and its maximum (i.e., 0) is achieved at the point $\hat{P}_{\mathrm{D}}=\hat{P}_{\mathrm{FA}}$. We further have $\beta_1(\hat{P}_{\mathrm{D}})\leq 0$ and $\frac{\mathrm{d}\beta(\hat{P}_{\mathrm{D}})}{\mathrm{d}\hat{P}_{\mathrm{D}}}\leq 0$. Thus, $\beta(\hat{P}_{\mathrm{D}})$ decreases as $\hat{P}_{\mathrm{D}}$ increases. ■

B. Proof of **Lemma** 2

Based on **Lemma** 1, $\left\lceil \frac{R+1}{1+\beta(\hat{P}_{\mathrm{D}})} \right\rceil$ follows a stepwise ascent as $\hat{P}_{\mathrm{D}}$ increases. We first define $\hat{P}_{\mathrm{D}}^{\tilde{\kappa},\min}$ and $\hat{P}_{\mathrm{D}}^{\tilde{\kappa},\max}$, which satisfy

$$\hat{P}_{\mathrm{D}}^{\tilde{\kappa},\min} = \arg\min_{\hat{P}_{\mathrm{D}}} \left[\min\left(R+1, \left\lceil \frac{R+1}{1+\beta(\hat{P}_{\mathrm{D}})} \right\rceil\right) = \tilde{\kappa} \right], \tag{56}$$

and

$$\hat{P}_{\mathrm{D}}^{\tilde{\kappa},\max} = \arg\max_{\hat{P}_{\mathrm{D}}} \left[\min\left(R+1, \left\lceil \frac{R+1}{1+\beta(\hat{P}_{\mathrm{D}})} \right\rceil\right) = \tilde{\kappa} \right], \tag{57}$$

respectively. κ is a constant and equal to $\tilde{\kappa}$ when $\hat{P}_{\mathrm{D}} \in [\hat{P}_{\mathrm{D}}^{\kappa,\tilde{\min}}, \hat{P}_{\mathrm{D}}^{\kappa,\tilde{\max}}]$. We will prove **Lemma** 2 in two steps. Specifically, we first prove that the probability of error $\Upsilon(\kappa, \hat{P}_{\mathrm{D}})$ at the FC decreases as $\hat{P}_{\mathrm{D}}$ increases when $\hat{P}_{\mathrm{D}}^{\tilde{\kappa}} \in (\hat{P}_{\mathrm{D}_{\min}}^{\tilde{\kappa}}, \hat{P}_{\mathrm{D}_{\max}}^{\tilde{\kappa}}]$. In such a case, $\tilde{\kappa}$ is fixed and equal to $\tilde{\kappa}$ and $\Upsilon(\kappa, \hat{P}_{\mathrm{D}})$ can be simplified as

$$\Upsilon_1(\hat{P}_{\mathrm{D}}) = \frac{1}{2}\sum_{i=0}^{\tilde{\kappa}-1} \binom{R+1}{i} (\hat{P}_{\mathrm{D}})^i (1-\hat{P}_{\mathrm{D}})^{R+1-i}, \tag{58}$$

which decreases as $\hat{P}_{\mathrm{D}}$ increases. This is because the CDF of the binomial distribution $\Upsilon_1(\hat{P}_{\mathrm{D}})$ can be represented in terms of the regularized incomplete beta function [36]:

$$\Upsilon(\hat{P}_{\mathrm{D}}) = (R+2-\tilde{\kappa}) \binom{R+1}{i} \int_0^{1-\hat{P}_{\mathrm{D}}} t^{R+1-\tilde{\kappa}} (1-t)^{\tilde{\kappa}-1} \mathrm{d}t,$$

whose derivative meets the following constraint,

$$\frac{\mathrm{d}\Upsilon(\hat{P}_{\mathrm{D}})}{\mathrm{d}\hat{P}_{\mathrm{D}}} = -(R+2-\tilde{\kappa}) \binom{R+1}{i} (1-\hat{P}_{\mathrm{D}})^{R+1-\tilde{\kappa}} (\hat{P}_{\mathrm{D}})^{\tilde{\kappa}-1} \leq 0. \tag{59}$$

Secondly, we prove that the probability of error $\Upsilon(\kappa, \hat{P}_{\mathrm{D}})$ at the FC decreases when κ varies from $\tilde{\kappa}$ to $\tilde{\kappa}+1$ due to the increase of $\hat{P}_{\mathrm{D}}$. According to (56) and (57), we have

$$\begin{aligned}
&\Upsilon(\tilde{\kappa}+1, \hat{P}_{\mathrm{D}}^{\tilde{\kappa}+1,\min}) - \Upsilon(\tilde{\kappa}, \hat{P}_{\mathrm{D}}^{\tilde{\kappa},\max}) \\
\leq &\Upsilon(\tilde{\kappa}+1, \hat{P}_{\mathrm{D}}^{\tilde{\kappa},\max}) - \Upsilon(\tilde{\kappa}, \hat{P}_{\mathrm{D}}^{\tilde{\kappa},\max}) \\
= &\binom{R+1}{\tilde{\kappa}} \left[(\hat{P}_{\mathrm{D}}^{\tilde{\kappa},\max})^{\tilde{\kappa}} (1-\hat{P}_{\mathrm{D}}^{\tilde{\kappa},\max})^{R+1-\tilde{\kappa}} - (\hat{P}_{\mathrm{FA}})^{\tilde{\kappa}} (1-\hat{P}_{\mathrm{FA}})^{R+1-\tilde{\kappa}} \right],
\end{aligned} \tag{60}$$

and

$$\tilde{\kappa} = \frac{R+1}{1+\beta(\hat{P}_{\mathrm{D}}^{\tilde{\kappa},\max})} = \frac{(R+1)\ln\frac{1-\hat{P}_{\mathrm{FA}}}{1-\hat{P}_{\mathrm{D}}^{\tilde{\kappa},\max}}}{\ln\frac{\hat{P}_{\mathrm{D}}^{\tilde{\kappa},\max}(1-\hat{P}_{\mathrm{FA}})}{\hat{P}_{\mathrm{FA}}(1-\hat{P}_{\mathrm{D}}^{\tilde{\kappa},\max})}}. \tag{61}$$

Then, substituting (61) into (60), we obtain

$$\Upsilon(\tilde{\kappa}+1, \hat{P}_{\mathrm{D}}^{\tilde{\kappa},\max}) - \Upsilon(\tilde{\kappa}, \hat{P}_{\mathrm{D}}^{\tilde{\kappa},\max}) = 0 \tag{62}$$

which suggests that $\Upsilon(\kappa, \hat{P}_{\mathrm{D}})$ decreases when κ varies from $\tilde{\kappa}$ to $\tilde{\kappa}+1$. Finally, we can conclude that $\Upsilon(\kappa, \hat{P}_{\mathrm{D}})$ decreases as $\hat{P}_{\mathrm{D}}$ increases in the whole feasible region $\hat{P}_{\mathrm{D}} \in (0,1)$. ■

*C. Proof of **Lemma** 3*

Since $\hat{P}_{\mathrm{D}}$ is the average of P_{D_r} and P_{D_r} is a monotonically increasing function with respect to ρ_r [28], we just need to prove that ρ_r increases as p_0 increases. It is observed that $\mathrm{tr}(\mathbf{Q}_r + \sigma_{\mathrm{n}}^2\mathbf{I}_{N_1})$ is a constant associated with $P_{\max}$, thus it can be approximated as

$$\mathrm{tr}(\mathbf{Q}_r + \sigma_{\mathrm{n}}^2\mathbf{I}_{N_1}) \simeq \mathrm{tr}(\hat{\mathbf{W}}), \tag{63}$$

where $\simeq$ represents the same trend with respect to the variation of p_0 on the left-hand and right-hand sides. We also have

$$\begin{aligned} \mathrm{tr}\left(\mathbf{B}_r\hat{\mathbf{W}}\hat{\mathbf{W}}^H\mathbf{B}_r^H\right) &= \mathrm{tr}\left(\hat{\mathbf{W}}\hat{\mathbf{W}}^H\mathbf{a}(\theta)\mathbf{b}_1^H(\varphi_r)\mathbf{b}_1(\varphi_r)\mathbf{a}^H(\theta)\right) \\ &\simeq \mathrm{tr}\left(\hat{\mathbf{W}}\hat{\mathbf{W}}^H\mathbf{a}(\theta)\mathbf{a}^H(\theta)\right). \end{aligned} \tag{64}$$

Then,

$$\begin{aligned} \rho_r &\simeq \mathrm{tr}\left(\frac{\mathbf{B}_r\hat{\mathbf{W}}\hat{\mathbf{W}}^H\mathbf{B}_r^H}{\mathbf{Q}_r + \sigma_{\mathrm{n}}^2\mathbf{I}_{N_1}}\right) \\ &\simeq \mathrm{tr}\left(\frac{\hat{\mathbf{W}}\hat{\mathbf{W}}^H\mathbf{a}(\theta)\mathbf{a}^H(\theta)}{\hat{\mathbf{W}}}\right) \\ &= \mathrm{tr}\left(\mathrm{diag}(\mathbf{p})\tilde{\mathbf{W}}^H\mathbf{a}(\theta)\mathbf{a}^H(\theta)\tilde{\mathbf{W}}\right), \end{aligned} \tag{65}$$

it is obvious that $\tilde{\mathbf{w}}_0^H\mathbf{a}(\theta) > \tilde{\mathbf{w}}_i^H\mathbf{a}(\theta)$ due to the ZFR precoder in (10). Thus, ρ_r increases as p_0 increases. ■

REFERENCES

[1] Z. Zhang, Y. Xiao, Z. Ma, M. Xiao, Z. Ding, X. Lei, G. K. Karagiannidis, and P. Fan, "6G wireless networks: Vision, requirements, architecture, and key technologies," *IEEE Trans. Veh. Technol.*, vol. 14, no. 3, pp. 28–41, July 2019.

[2] A. Hassanien, M. G. Amin, Y. D. Zhang, and F. Ahmad, "Dual-function radar-communications: Information embedding using sidelobe control and waveform diversity," *IEEE Trans. Signal Process.*, vol. 64, no. 8, pp. 2168–2181, Apr. 2016.

[3] F. Liu, C. Masouros, A. P. Petropulu, H. Griffiths, and L. Hanzo, "Joint radar and communication design: Applications, state-of-the-art, and the road ahead," *IEEE Trans. Commun.*, vol. 68, no. 6, pp. 3834–3862, Jun. 2020.

[4] J. A. Zhang, M. L. Rahman, X. Huang, Y. J. Guo, S. Chen, and R. W. Heath, "Perceptive mobile networks: Cellular networks with radio vision via joint communication and radar sensing," *IEEE Veh. Technol. Mag.*, vol. 16, no. 2, pp. 20–30, June 2021.

[5] J. A. Zhang, M. L. Rahman, K. Wu, X. Huang, Y. J. Guo, S. Chen, and J. Yuan, "Enabling joint communication and radar sensing in mobile networks-A survey," *IEEE Commun. Surveys Tuts.*, vol. 24, no. 1, pp. 306–345, Feb. 2022.

[6] T. Wild, V. Braun, and H. Viswanathan, "Joint design of communication and sensing for beyond 5G and 6G systems," *IEEE Access*, vol. 9, pp. 30 845–30 857, Feb. 2021.

[7] J. A. Zhang, K. Wu, X. Huang, Y. J. Guo, D. Zhang, and R. W. Heath, "Integration of radar sensing into communications with asynchronous transceivers," *IEEE Commun. Mag.*, vol. 60, no. 11, pp. 106–112, Nov. 2022.

[8] D. K. Pin Tan, J. He, Y. Li, A. Bayesteh, Y. Chen, P. Zhu, and W. Tong, "Integrated sensing and communication in 6g: Motivations, use cases, requirements, challenges and future directions," in *Proc. 1st IEEE Int. Online Symp. Joint Commun. Sens.(JC&S), Dresden, Germany*, Feb. 2021, pp. 1–6.

[9] B. J. Donnet and I. D. Longstaff, "Combining MIMO radar with OFDM communications," in *Proc. European Radar Conf. (EURAD), Manchester, UK*, Sep. 2006, pp. 37–40.

[10] F. Liu, C. Masouros, A. Li, H. Sun, and L. Hanzo, "MU-MIMO communications with MIMO radar: From co-existence to joint transmission," *IEEE Trans. Wireless Commun.*, vol. 17, no. 4, pp. 2755–2770, Apr. 2018.

[11] X. Liu, T. Huang, N. Shlezinger, Y. Liu, J. Zhou, and Y. C. Eldar, "Joint transmit beamforming for multiuser MIMO communications and MIMO radar," *IEEE Trans. Signal Process.*, vol. 68, pp. 3929–3944, Jun. 2020.

[12] F. Liu, Y.-F. Liu, A. Li, C. Masouros, and Y. C. Eldar, "Cramér-rao bound optimization for joint radar-communication beamforming," *IEEE Trans. Signal Process.*, vol. 70, pp. 240–253, Feb. 2022.

[13] K. Wu, J. A. Zhang, X. Huang, Y. J. Guo, and R. W. Heath, "Waveform design and accurate channel estimation for frequency-hopping mimo radar-based communications," *IEEE Trans. Commun.*, vol. 69, no. 2, pp. 1244–1258, Feb. 2021.

[14] Z. Ni, J. A. Zhang, X. Huang, K. Yang, and J. Yuan, "Uplink sensing in perceptive mobile networks with asynchronous transceivers," *IEEE Trans. Signal Process.*, vol. 69, pp. 1287–1300, Feb. 2021.

[15] A. Chowdary, A. Bazzi, and M. Chafii, "On hybrid radar fusion for integrated sensing and communication," *arXiv preprint arXiv:2303.05722*, 2023.

[16] D. Xu, C. Liu, S. Song, and D. W. K. Ng, "Integrated sensing and communication in coordinated cellular networks," *arXiv preprint arXiv:2305.01213*, 2023.

[17] S. Z. Gurbuz and M. G. Amin, "Radar-based human-motion recognition with deep learning: Promising applications for indoor monitoring," *IEEE Signal Process. Mag.*, vol. 36, no. 4, pp. 16–28, July 2019.

[18] H. Godrich, A. M. Haimovich, and R. S. Blum, "Target localization accuracy gain in mimo radar-based systems," *IEEE Trans. Inf. Theory*, vol. 56, no. 6, pp. 2783–2803, June 2010.

[19] Z. Behdad, Ö. T. Demir, K. W. Sung, E. Björnson, and C. Cavdar, "Power allocation for joint communication and sensing in cell-free massive MIMO," *arXiv preprint arXiv:2209.01864*, 2022.

[20] V. Yajnanarayana and H. Wymeersch, "Multistatic sensing of passive targets using 6G cellular infrastructure," *arXiv preprint arXiv:2211.05340*, 2022.

[21] Y. Huang, Y. Fang, X. Li, and J. Xu, "Coordinated power control for network integrated sensing and communication," *IEEE Trans. Veh. Technol.*, vol. 71, no. 12, pp. 13 361–13 365, Dec. 2022.

[22] G. Cheng and J. Xu, "Coordinated transmit beamforming for multi-antenna network integrated sensing and communication," *arXiv preprint arXiv:2211.01085*, 2022.

[23] G. Li, S. Wang, K. Ye, M. Wen, D. W. K. Ng, and M. Di Renzo, "Multi-point integrated sensing and communication: Fusion model and functionality selection," *IEEE Wireless Commun. Lett.*, vol. 11, no. 12, pp. 2660–2664, 2022.

[24] F. Liu, C. Masouros, A. Li, T. Ratnarajah, and J. Zhou, "MIMO radar and cellular coexistence: A power-efficient approach enabled by interference exploitation," *IEEE Trans. Signal Process.*, vol. 66, no. 14, pp. 3681–3695, July 2018.

[25] N. Zhao, Y. Wang, Z. Zhang, Q. Chang, and Y. Shen, "Joint transmit and receive beamforming design for integrated sensing and communication," *IEEE Commun. Lett.*, vol. 26, no. 3, pp. 662–666, Mar. 2022.

[26] S. Buzzi, C. D' Andrea, and M. Lops, "Using massive MIMO arrays for joint communication and sensing," in *Proc. IEEE Asilomar Conf. Signals, Syst., Comput., Pacific Grove, CA, USA*, 2019, pp. 5–9.

[27] B. Li and A. P. Petropulu, "Joint transmit designs for coexistence of MIMO wireless communications and sparse sensing radars in clutter," *IEEE Trans. Aerosp. Electron. Syst.*, vol. 53, no. 6, pp. 2846–2864, Dec. 2017.

[28] S. Kay and P. Hall, *Fundamentals of Statistical Signal Processing, Volume II:Detection Theory*. Englewood Cliffs, NJ: Prentice-Hall, 1993.

[29] Q. He, N. H. Lehmann, R. S. Blum, and A. M. Haimovich, "MIMO radar moving target detection in homogeneous clutter," *IEEE Trans. Aerosp. Electron. Syst.*, vol. 46, no. 3, pp. 1290–1301, July 2010.

[30] I. Bekkerman and J. Tabrikian, "Target detection and localization using MIMO radars and sonars," *IEEE Trans. Signal Process.*, vol. 54, no. 10, pp. 3873–3883, Oct 2006.

[31] S. Boyd, S. P. Boyd, and L. Vandenberghe, *Convex optimization*. Cambridge university press, 2004.

[32] A. Khawar, A. Abdelhadi, and C. Clancy, "Target detection performance of spectrum sharing MIMO radars," *IEEE Sensors J.*, vol. 15, no. 9, pp. 4928–4940, Sep. 2015.

[33] P. K. Varshney, *Distributed Detection and Data Fusion*. New York: Springer-Verlag, 1997.

[34] W. Xia, G. Zheng, Y. Zhu, J. Zhang, J. Wang, and A. P. Petropulu, "A deep learning framework for optimization of MISO downlink beamforming," *IEEE Trans. Commun.*, vol. 68, no. 3, pp. 1866–1880, Mar. 2020.

[35] J. L. Eaves and E. K. Reedy, *Principles of Modern Radar*. New York: Van Nostrand Reinhold, 1987.

[36] G. P. Wadsworth, J. G. Bryan, and A. C. Eringen, "Introduction to probability and random variables," *Tech. Rep.*, vol. 28, no. 2, p. 319, 1961.